Proceedings of the Combustion Institute 42 (2026) 106758

Contents lists available at ScienceDirect

Proceedings of the Combustion Institute

journal homepage: www.elsevier.com/locate/proci

# Investigation of ignition delay times of oxygen-enriched methane mixtures using a rapid compression machine

Sara Spano [a,b], Florian Hurault [c], Fabrice Foucher [c], Alessandro Parente [b,d,e], Axel Coussement [b,d], Francesco Contino [a], Hervé Jeanmart [a], Yuki Murakami [b,d,e,*]

[a] Université catholique de Louvain, Institute of Mechanics, Materials and Civil Engineering, Louvain-la-Neuve, Belgium
[b] Université Libre de Bruxelles, École polytechnique de Bruxelles, Aero-Thermo-Mechanics Laboratory, Brussels, Belgium
[c] Université d'Orléans, PRISME Laboratory, France
[d] Brussels Institute for Thermal-Fluid Systems and Clean Energy (BRITE), Université Libre de Bruxelles and Vrije Universiteit Brussel, Belgium
[e] WEL Research Institute, Belgium

ARTICLE INFO

*Keywords:*
Ignition
Natural gas
Chemical kinetics
Oxy-fuel combustion
Methylperoxy radicals

ABSTRACT

This work investigates the effects of oxygen ($O_2$) enrichment on ignition delay times of methane ($CH_4$) using a rapid compression machine (RCM) at low-to-intermediate temperatures and high-pressure conditions, aiming at internal combustion engine applications. $O_2$ percentages in the oxidiser range from 21% to 100% at a fixed fuel volume. Experimental measurements indicate that the ignition delay times of $CH_4$ monotonically decrease as the $O_2$ concentration increases at a fixed temperature. To accurately simulate the ignition phenomena of $O_2$-enriched mixtures in a RCM, a "pseudo" non-reactive pressure–time history, created based on reactive test data, is used to consider the facility effects. By using the simulation input based on a pseudo non-reactive pressure profile, the ignition delay times are accurately simulated with a recent detailed chemical kinetic mechanism. Chemical kinetic analyses reveal that the observed enhancement in mixture reactivity is due to strengthened pathways involving methylperoxy radicals ($CH_3\dot{O}_2$). The findings obtained in the present study advance the application of $O_2$-enriched $CH_4$ combustion and the ignition control for practical internal combustion engines.
*Novelty and significance statement:* The present work makes three main contributions: (1) a new set of ignition delay time (IDT) measurements for $CH_4$ mixtures at $O_2$-enriched conditions; (2) the demonstration of the RCM simulations using a "pseudo" non-reactive pressure–time history; and (3) a detailed chemical kinetic analysis of $O_2$-enriched $CH_4$ combustion without dilution at engine-relevant conditions. First, this study presents experimental and numerical investigations of IDTs for $O_2$-enriched $CH_4$ mixtures for the conditions which have scarcely been examined using RCMs. The new experimental datasets extend the benchmarks for validation and further development of chemical kinetic mechanisms. Second, the introduction of a pseudo non-reactive pressure profile in RCM simulation is key to accurately consider the facility effects, especially when the $O_2$ concentration in the oxidizer is varied. The proposed approach is broadly applicable to RCM studies involving variations in oxidizer composition. Third, the chemical kinetic analysis clarifies the mechanisms responsible for the enhanced reactivity of $CH_4$ mixtures for oxy-fuel conditions across a wide range of $O_2$ concentrations, providing insights relevant to high-compression-ratio, low-temperature combustion engine applications.

## 1. Introduction

With the climate crisis accelerating, decarbonising internal combustion engines — which still supply a substantial share of global energy conversion — demands technologies that raise thermal efficiency while curbing fuel-borne $CO_2$. Homogeneous Charge Compression Ignition (HCCI) engines are considered promising candidate: by enabling spatially uniform heat release at comparatively low temperatures, it approaches thermodynamic-limit efficiencies with suppressed NOx and particulate matter [1]. Methane ($CH_4$) couples anti-knock resilience with a high H/C ratio, enabling higher-compression, lean operation and reduced $CO_2$ and pollutant emissions [2]. Additionally, power-to-methane pathways integrate it into a decarbonised fuel supply. Such combustion properties of $CH_4$ align with HCCI engines, promising high efficiency with low pollutant emissions. However, the major challenge is ignition control: whereas conventional higher hydrocarbons can suffer pre-ignition owing to complex low-temperature chemistry [3],

* Corresponding author.
*E-mail address:* murakami.yuki.4u@kyoto-u.ac.jp (Y. Murakami).

https://doi.org/10.1016/j.proci.2026.106758
Received 15 March 2026; Accepted 17 June 2026
Available online 28 October 2026
1540-7489/© 2026 The Combustion Institute. Published by Elsevier Inc. All rights are reserved, including those for text and data mining, AI training, and similar technologies.

the practical hurdle of $CH_4$ is its high auto-ignition temperature. $O_2$-enriched combustion offers a remedy, strengthening fuel oxidation to secure ignition for fuel-lean mixtures while allowing dilution to temper excessive pressure rise [4].

While $CH_4$ reactivity has been extensively studied over many years [5–8], investigations specifically targeting the low-temperature, high-pressure regime under oxygen-enriched conditions — i.e., the operating conditions considered in this work — remain limited. Panigrahy et al. [9] investigated ignition delay times of $H_2/CH_4$ blends in the RCM experiment. They confirmed that at temperature below 900 K, $H\dot{O}_2$ chemistry dominates fuel oxidation and the active involvement of $CH_3\dot{O}_2$ in $H\dot{O}_2$ consumption affects the mixture reactivity. Harman-Thomas et al. [10] also reported that chemical kinetic mechanisms lacking $CH_3\dot{O}_2$ tend to overpredict fuel reactivity, especially at elevated pressures. Many investigations on $CH_3\dot{O}_2$ chemistry are based on sub-atmospheric pressure conditions [11–14], and there remains large uncertainties in reactions involving $CH_3\dot{O}_2$, especially at elevated pressures.

Motivated by the discussion above, this study aims to elucidate the chemical kinetic mechanisms that govern $CH_4$ reactivity at low-to-intermediate temperatures and elevated pressures, especially at $O_2$-enriched and fuel-lean conditions. Ignition delay times of $CH_4$ are measured over a wide range of $O_2$-enrichment levels using a rapid compression machine (RCM). The experimental conditions were selected to be representative of the in-cylinder conditions encountered in high-compression-ratio engines operated in low-temperature combustion modes [4]. Furthermore, detailed chemical reaction analyses using a recent chemical kinetic mechanism are performed to identify the key reactions that control the $CH_4$ reactivity under the conditions of interest.

## 2. Experimental setup and methodology

### 2.1. Experimental setup

For the experimental measurements, the rapid compression machine (RCM) at the PRISME laboratory at Université d'Orléans was used. A detailed description of the experimental setup has been provided previously [15].

The $CH_4$ mole fraction was maintained constant at 3.05%, corresponding to a Fuel Mean Effective Pressure (FuelMEP) of 8 bar and an equivalence ratio ($\varphi$) of 0.3 in air (21% $O_2$). The compression temperature was varied by adjusting the initial gas temperature prior to compression. The initial temperature was adjusted by an external heater and controlled through an external wall-mounted temperature sensor. The initial temperature was monitored by a wall-mounted temperature sensor using a K-type thermocouple. The end-of-compression temperature ($T_c$) was varied between 900 K and 1030 K, while the end-of-compression pressure ($p_c$) was kept constant at 50 bar. The $O_2$ concentration in the oxidiser was varied in the range 21%–100%. At least three experimental runs were carried out for each $O_2$ concentration and temperature. The ignition delay time (IDT) was defined as the time interval between the end of compression and the point at which the rate of pressure rise reaches its maximum. The uncertainty in $T_c$ was estimated by propagating the individual sensor uncertainties through the isentropic relation following the methodology of Weber et al. [16], applied to all experimental measurements. The initial pressure $p_0$ was measured by a Keller PAA-33X static transducer (±0.1% FSO over a 5 bar range, $\sigma(p_0) = 0.0025$ bar), and the compressed pressure $p_c$ by a Kistler 6054BRU59 dynamic transducer (±0.3% FSO over a 300 bar range, $\sigma(p_c) = 0.45$ bar). The initial temperature $T_0$ was measured by a K-type thermocouple with ±2.5 K accuracy ($\sigma(T_0) = 1.25$ K). The dominant contributions to $\sigma(T_c)$ come from $T_0$ (amplified by the compression factor $\partial T_c/\partial T_0 \approx 2.0$ K/K, contributing ~2.5 K) and from $p_c$ (~2.0 K); the $p_0$ contribution is negligible (<0.03 K). The combined propagated uncertainty is $\pm\delta T_c\,(2\sigma) = 6.2$–$6.8$ K across the full dataset, with a mean of ±6.5 K. The shot-to-shot reproducibility of $T_c$ has a standard deviation of $\sigma \approx 1.0$ K (±2 K at $2\sigma$). The experimental conditions tested are summarised in Table 1.

**Table 1**
Experimental test matrix for ignition delay time measurements of $CH_4/O_2/N_2$ mixtures in the rapid compression machine.

| $O_2$ in oxidizer [%] | $X_{CH_4}$ [–] | $X_{O_2}$ [–] | $X_{N_2}$ [–] | $\phi$ [–] | $p_c$ (bar) | $T_c$ (K) |
|---|---|---|---|---|---|---|
| 21 | 0.0305 | 0.2036 | 0.7659 | 0.300 | 50 | 900–1000 |
| 30 | 0.0305 | 0.2909 | 0.6786 | 0.210 | 50 | 925–1030 |
| 45 | 0.0305 | 0.4363 | 0.5332 | 0.140 | 50 | 925–1000 |
| 50 | 0.0305 | 0.4848 | 0.4847 | 0.126 | 50 | 900–1000 |
| 55 | 0.0305 | 0.5332 | 0.4363 | 0.114 | 50 | 900–1000 |
| 60 | 0.0305 | 0.5817 | 0.3878 | 0.105 | 50 | 900–1000 |
| 70 | 0.0305 | 0.6787 | 0.2908 | 0.090 | 50 | 900–1000 |
| 80 | 0.0305 | 0.7756 | 0.1939 | 0.079 | 50 | 900–1000 |
| 90 | 0.0305 | 0.8725 | 0.0970 | 0.070 | 50 | 900–975 |
| 100 | 0.0305 | 0.9695 | 0.0000 | 0.063 | 50 | 900–975 |

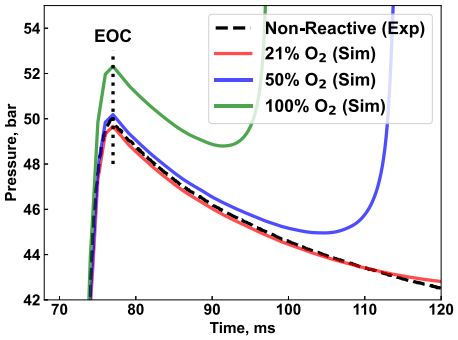



**Fig. 1.** Pressure–time histories of reactive tests based on non-reactive simulation input for $O_2$ 21%–100%.

The Fuel Mean Effective Pressure (FuelMEP) was defined as the chemical energy of the fuel charge per unit displaced volume:

$$\text{FuelMEP} = \frac{\text{LHV} \cdot m_f}{V_d} \tag{1}$$

where LHV is the lower heating value of methane ($\text{LHV}_{CH_4} = 50.05$ MJ/kg), $m_f$ is the mass of fuel in the combustion chamber, and $V_d$ is the displaced volume of the RCM. A FuelMEP of 8 bar corresponds to a $CH_4$ mole fraction of 3.05% at the initial conditions of the present experiments.

### 2.2. Numerical simulations using "pseudo" non-reactive pressure profiles

Numerical simulations and reaction analyses were performed using a 0-D homogeneous reactor model in Cantera v3.0.0 [17]. The C3Mech-LiteV4.0.1 model (H2-CH4_36sp) [18,19], the FFCM-2 model [20] and the ThInK1.0 model [21] are used for the comparison, which are recently published mechanisms and validated against a wide range of validation targets, especially small hydrocarbon fuels.

When accounting for facility effects in ignition delay time measurements using a RCM, a non-reactive pressure profile is measured by replacing $O_2$ in the mixture with an inert gas such as $N_2$. By using a volume-time profile derived from this non-reactive pressure profile as an input for numerical simulations, the facility-dependent effects, such as heat losses to the walls, are incorporated.

However, this approach holds at the conditions that thermochemical properties of the mixture remain consistent (or similar) between the reactive and the non-reactive mixtures where $O_2$ is replaced by an inert gas. The effects of changes in mixture thermal properties due to the $O_2$ substitution on the pressure and temperature profiles cannot be

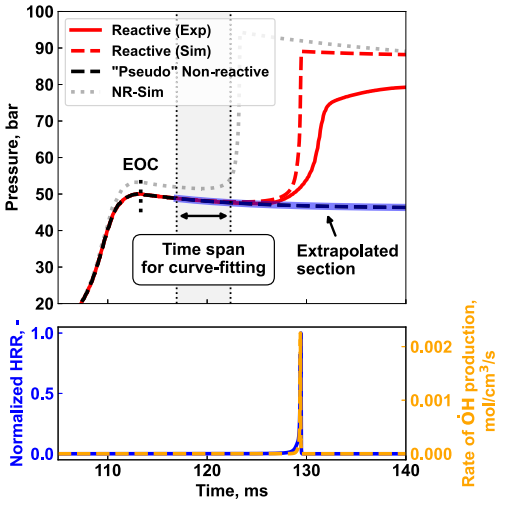



**Fig. 2.** (Top) Comparison of the measured and simulated pressure–time histories for the $O_2$ 100% case ($p_c$ = 50 bar, $T_c$ = 950 K): the measured pressure profile (red solid line); the simulated pressure profile based on the pseudo pressure profile (red dashed line); the pseudo non-reactive pressure profile (black dashed line); the simulated pressure profile based on a non-reactive pressure profile (gray dotted line). The time span between the 20% and 50% IDTs were used to generate a pseudo pressure profile. (Bottom) The normalised heat release rate and the rate of ȮH production profiles.

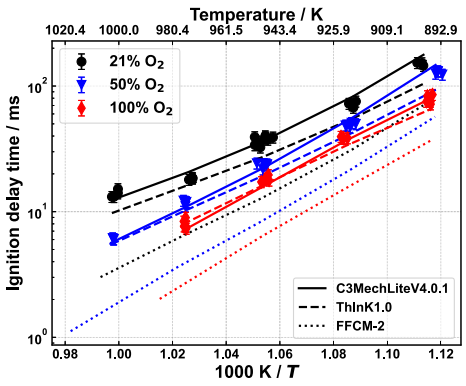



**Fig. 3.** Measured and computed IDTs of $CH_4/O_2/N_2$ mixtures at 50 bar with 21%–100% $O_2$.

neglected, particularly under the conditions where the $O_2$ mole fraction in the oxidizer is varied over a wide range (21%–100%), as in this study. Fig. 1 shows the pressure–time profiles obtained from simulations of reactive mixture conditions with varying $O_2$ fractions, based on the non-reactive pressure profile for a $CH_4/N_2$ mixture. Focusing on the profiles near the end-of-compression (EOC), it is evident that the simulated profiles do not perfectly overlap with the non-reactive pressure profile at any $O_2$ concentration. Notably, in the 100% $O_2$ case, the pressure reached at EOC is significantly overestimated.

To address this issue, this study introduces an approach to create a "pseudo" non-reactive pressure profile by utilising and extrapolating a portion of the post-EOC data from the reactive pressure profile. The decreases in pressure and temperature due to heat transfer to the walls of the RCM combustion chamber in the post-EOC region generally exhibit an exponential decay. Therefore, a curve-fitting to the following exponential decay function was performed using the pressure data from the time span corresponding to 20%–50% of the total IDT:

$$p(t) = a \cdot e^{-b \cdot t} + c \tag{2}$$

Here, $p(t)$ is the pressure at time $t$, and $a$, $b$, and $c$ are fitting parameters. The pseudo non-reactive pressure profile was generated by extrapolating the obtained fitted curve to the time period after ignition. In principle, a generated pseudo non-reactive pressure trace must coincide with, but never exceed, the original reactive pressure trace within the induction period. When the start of the time window is fixed at the 0%–20% IDT interval, or the end of the window is set at the 30%–40% IDT interval, the pseudo pressure trace tends to rise above the original one. Because a reactive pressure profile usually begins to increase exponentially from roughly the 60%–70% IDT interval, the end of the selected time window was restricted to the 50% IDT. Based on these results, the 20%–50% IDT interval was selected. The rationale for this time window is presented in Supplementary Material. Additionally, a sensitivity analysis was conducted to evaluate the effects of an interval selection on IDTs. Two intervals, the 20%–50% IDT and 30%–50% IDT intervals, were tested. We confirmed that the difference between these two intervals results in ±3% differences in the simulated IDTs.

All the numerical simulations in this study are performed using the volume-time profile generated based on this pseudo non-reactive pressure profile as the input, regardless of $O_2$ concentrations. This approach enables to accurately capture the facility effects while eliminating errors caused by the inconsistent thermochemical properties of test mixtures. Conceptually, the procedure is analogous to the treatment in shock tube studies considering a pressure increase prior to ignition, where the experimentally observed pressure history is incorporated to reconstruct the thermodynamic trajectory experienced by a mixture prior to ignition [22,23].

In Fig. 2, four pressure traces are shown for the 100% $O_2$ case ($p_c$ = 50 bar, $T_c$ = 950 K): a pseudo non-reactive pressure trace (black dashed line), the measured reactive pressure trace (red solid line), a simulated pressure trace based on the pseudo profile (red dashed line, using C3MechV4.0.1), and a simulated pressure trace based on a purely non-reactive pressure profile (grey dotted line). The segment of the experimental reactive pressure curve within the grey-shaded area was used to construct the pseudo non-reactive profile. Whereas the simulation using the non-reactive profile substantially overpredicts $p_c$ at EOC, the simulated profiles derived from the pseudo curve closely reproduce the measured pressure profile in both the pre- and post-EOC regions. Fig. 2 also includes the normalised heat release rate and the rate of ȮH production profiles. The absence of appreciable heat release and ȮH radical formation during the induction period indicates that the influence of chemical reactions on the pseudo-pressure curve is negligible. The measured IDT data and the input files in Chemkin format are provided in Supplementary Material.

## 3. Results and discussion

### 3.1. Experimental results

Fig. 3 presents the comparison of measured and computed IDTs of $CH_4/O_2/N_2$ mixtures at $p_c$ = 50 bar and $T_c$ = 900–1000 K with the $O_2$ concentrations varying in the range 21%–100%. Measured IDTs clearly indicate that IDTs decrease as the $O_2$ concentration increases. Computed IDTs with three different models also capture this general trend. The C3MechLiteV4.0.1 model shows good agreement with the measurements at different $O_2$ concentrations, while the ThInK1.0 model predicts slightly shorter IDTs under 21% and 50% $O_2$ conditions, with a maximum discrepancies of 30% and 27%, respectively. The FFCM-2 model tends to predict significantly shorter IDTs. The large discrepancies in the predictions by the FFCM-2 model stem from the inclusion of the reaction $CH_3\dot{O}_2 + O_2 = CH_2O + \dot{O}H + O_2$, employing the rate constant proposed by Lakshmanan et al. [24]. The FFCM-2 model includes the reaction to improve the predictions of IDTs of $CH_4$ mixtures for high pressure and high oxygen concentration conditions,

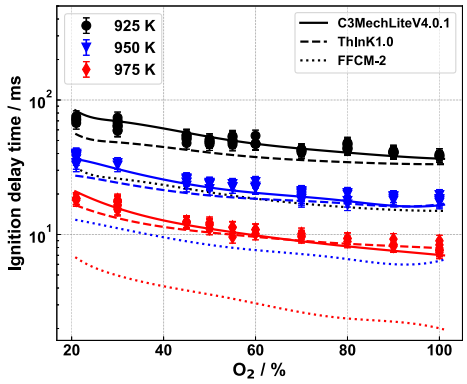



**Fig. 4.** Dependence of IDTs of $CH_4/O_2/N_2$ mixtures on the $O_2$ concentration at 925–975 K.

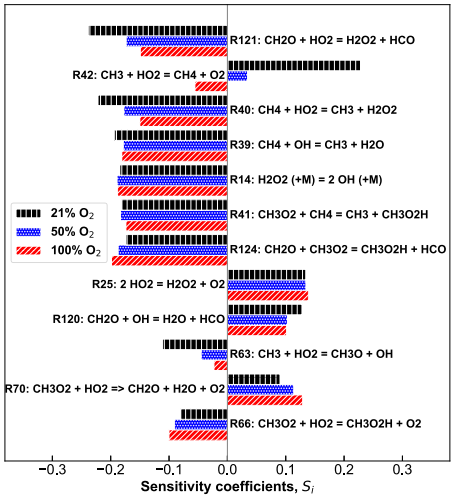



**Fig. 5.** IDT sensitivity for $CH_4/O_2/N_2$ mixtures at 50 bar and 925 K with $O_2$ concentration 21%–100%.

measured in the Shock Tube (ST) experiments by Shao et al. [25] and Karimi et al. [26]. While including this reaction improves predictions for the ST measurements, it largely underestimates the IDTs measured in RCMs. This reaction greatly modifies the reactivity of $CH_4$ mixtures, especially for $O_2$-enriched conditions, as it is very sensitive to $O_2$ concentration and it generates $\dot{O}H$ radicals. In fact, if this reaction is removed, the predictions by the FFCM-2 model become closer to the other mechanisms' predictions. Fig. 4 presents the dependence of IDTs of $CH_4/O_2/N_2$ mixtures on $O_2$ concentrations 21%–100% at 925–975 K. At all temperatures considered, the measured IDTs become shorter as the $O_2$ concentration increases. The C3MechLiteV4.0.1 model captures well the IDT dependence on $O_2$ concentrations at different temperatures. The ThInK1.0 model predicts slightly shorter IDTs at 925 K for different $O_2$ concentrations. The FFCM-2 model generally predicts shorter IDTs than the other mechanisms for these temperature and $O_2$ concentrations.

Based on these observations, the following sections address the mechanism for the reactivity enhancement with $O_2$ enrichment based on chemical reaction analyses using the C3MechLiteV4.0.1 model.

### 3.2. Effects of $O_2$ enrichment on $CH_4$ reactivity

To investigate the dominant reaction pathways governing the IDTs of $CH_4/O_2/N_2$ mixtures at various $O_2$ concentrations, a brute-force sensitivity analysis was performed. The sensitivity coefficients with respect to the IDTs were calculated using the following equation:

$$S_i = \frac{\ln(\tau_{2.0k_i}/\tau_{0.5k_i})}{\ln(2.0/0.5)}, \tag{3}$$

where $S_i$ and $k_i$ represent the sensitivity coefficient and rate constant of the $i_{\text{th}}$ reaction, respectively, and $\tau$ denotes the calculated IDT. A positive sensitivity coefficient indicates that the reaction inhibits the overall reactivity of the mixture, whereas a negative value implies a promoting effect.

Fig. 5 presents the sensitivity coefficients of the top sensitive reactions to IDTs of $CH_4/O_2/N_2$ mixtures at 50 bar and 925 K with 21%–100% $O_2$.

At the lowest $O_2$ concentration (21% $O_2$), R121: $CH_2O + H\dot{O}_2 = H_2O_2 + H\dot{C}O$ and $\dot{H}$ atom abstraction reactions, such as R40: $CH_4 + H\dot{O}_2 = \dot{C}H_3 + H_2O_2$ and R39: $CH_4 + \dot{O}H = \dot{C}H_3 + H_2O$, show large promoting effects on IDTs of $CH_4/O_2/N_2$ mixtures. As the $O_2$ concentration increases (50%–100% $O_2$), the reactions involving $CH_3\dot{O}_2$, such as R41: $CH_3\dot{O}_2 + CH_4 = \dot{C}H_3 + CH_3O_2H$ and R124: $CH_2O + CH_3\dot{O}_2 = CH_3O_2H + H\dot{C}O$, have a relatively higher sensitivity than R121 and R40. This trend indicates that the relative importance of $CH_3\dot{O}_2$ reaction pathways in promoting $CH_4$ reactivity becomes larger with increasing $O_2$ concentration.

Considering the mixture is already lean at 21% $O_2$, it is reasonable for reactions involving $CH_3\dot{O}_2$ to have a high sensitivity at a low $O_2$ concentration. As reported in [9], methyl hydroperoxide ($CH_3O_2H$) immediately decomposes into $CH_3\dot{O}$ and $\dot{O}H$ radicals, promoting the mixture reactivity. This is the primary reason for the increased reactivity with increased $O_2$ concentrations at the conditions studied.

Based on the flux analyses, it was found that approximately 70% of the production of $CH_3O_2H$ is explained by R66: $CH_3\dot{O}_2 + H\dot{O}_2 = CH_3O_2H + O_2$, regardless of the $O_2$ concentrations. R40 contributes indirectly to the reactivity by generating $\dot{C}H_3$ radicals as the source of $CH_3\dot{O}_2$. Similarly, R121 enhances the reactivity as $H\dot{C}O$ generates $H\dot{O}_2$ through $H\dot{C}O + O_2 = CO + H\dot{O}_2$. However, the impact of the reactions directly generating $CH_3O_2H$, such as R41 and R124, becomes even more important than R40 and R121 as the $O_2$ concentration increases.

It is also interesting that R42: $\dot{C}H_3 + H\dot{O}_2 = CH_4 + O_2$ shows a positive sensitivity at lower $O_2$ concentrations (21%–50% $O_2$) but a negative sensitivity at a high $O_2$ concentration (100% $O_2$). At high $O_2$ levels, the increased $O_2$ availability enhances the regeneration of $\dot{C}H_3 + H\dot{O}_2$, thereby affecting the radical pool and mixture reactivity. This leads the competition for $CH_4$ between R40 and other reactions such as R39 and R41, resulting in a non-monotonic trend in those sensitivity coefficients.

To unveil the $CH_4$ chemistry dominating mixture reactivity, a reaction flux analysis was performed. Fig. 6 shows the $CH_4$ oxidation pathways for 50 bar and 925 K at elevated $O_2$ concentrations at the 20% $CH_4$ consumption. The black solid arrows and associated values correspond to species consumption, and grey dashed arrows and associated values correspond to species production (specifically for $\dot{O}H$, $H\dot{O}_2$, $H_2O_2$). The reaction pathways with noticeable changes are highlighted. In Fig. 6, it is evident that large changes are observed mostly upstream of $CH_2O$. Looking at the consumption of $\dot{C}H_3$, the reaction $\dot{C}H_3 + H\dot{O}_2 = CH_3\dot{O} + \dot{O}H$ has a large contribution at 21% $O_2$, however, the contribution decreases as the $O_2$ concentration increases. On the other hand, the contribution of $\dot{C}H_3 + O_2$ (+M) = $CH_3\dot{O}_2$ (+M) largely increases with increasing the $O_2$ concentration, and the subsequent pathway from $CH_3\dot{O}_2$ to $CH_3O_2H$ is also strengthened. As mentioned earlier, $CH_3O_2H$ immediately decomposes and supplies $\dot{O}H$ through $CH_3O_2H$ (+M) = $CH_3\dot{O} + \dot{O}H$ (+M), promoting the mixture reactivity. This trend is also obvious in the $\dot{O}H$ production. While the OH production from $\dot{C}H_3 + H\dot{O}_2 = CH_3\dot{O} + \dot{O}H$ decreases as the $O_2$ concentration increases, that from $CH_3O_2H$ (+M) = $CH_3\dot{O} + \dot{O}H$ (+M) increases greatly.

As for the reaction pathway from $CH_3\dot{O}$ to $\dot{O}H$, the contribution of the reaction $CH_3\dot{O}$ (+M) = $CH_2O + \dot{H}$ (+M) to the $CH_3\dot{O}$ consumption

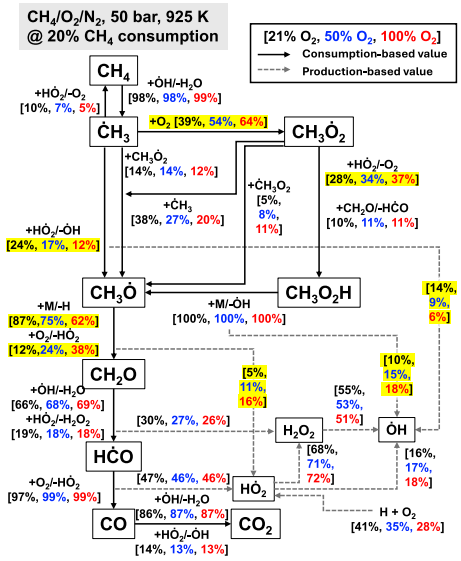



**Fig. 6.** Flux analysis on $CH_4$ oxidation at 50 bar and 925 K with 21%–100% $O_2$, at the 20% $CH_4$ consumption.

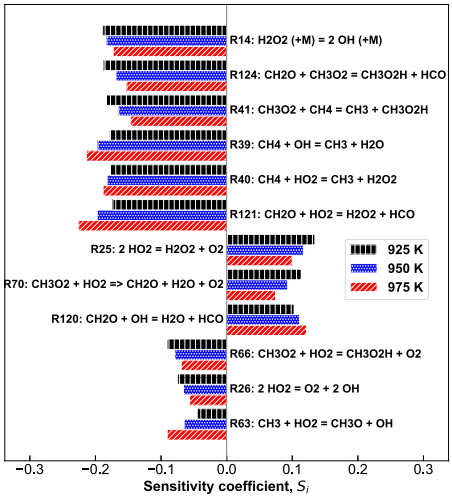



**Fig. 7.** IDT sensitivity for $CH_4/O_2/N_2$ mixtures at 50 bar and 925–975 K with 50% $O_2$.

decreases as $O_2$ increases, while that of the reaction $CH_3\dot{O} + O_2 = CH_2O + H\dot{O}_2$ increases, contributing to the $H\dot{O}_2$ production. $H\dot{O}_2$ also helps the conversion from $CH_3\dot{O}_2$ to $CH_3O_2H$, promoting the $\dot{O}H$ production through $CH_3O_2H$ (+M) = $CH_3\dot{O}$ + $\dot{O}H$ (+M). Therefore, the reactivity enhancement by $O_2$ enrichment is mainly due to the strengthened oxidation of $CH_4$ through the consecutive pathway: $CH_4 \rightarrow \dot{C}H_3 \rightarrow CH_3\dot{O}_2 \rightarrow CH_3O_2H \rightarrow CH_3\dot{O}$, and the active radical production through $CH_3O_2H$ (+M) = $CH_3\dot{O}$ + $\dot{O}H$ (+M).

### 3.3. Effects of temperature on $CH_4$ reaction pathway

As seen in Figs. 3 and 4, IDTs of $CH_4/O_2/N_2$ mixtures decrease as $T_c$ increases. A brute-force sensitivity analysis was performed in the same manner as Fig. 5 to identify the dominant reaction pathways governing the IDTs of $CH_4/O_2/N_2$ mixtures at different temperatures. Fig. 7 presents the sensitivity coefficients of the top sensitive reactions to IDTs of $CH_4/O_2/N_2$ mixtures (50 bar and 50% $O_2$) at $T_c$ = 925–975 K. It is interesting that the sensitivities of the reactions involving $CH_3\dot{O}_2$ decrease as the temperature increases (R124, R41, R70, R66), while

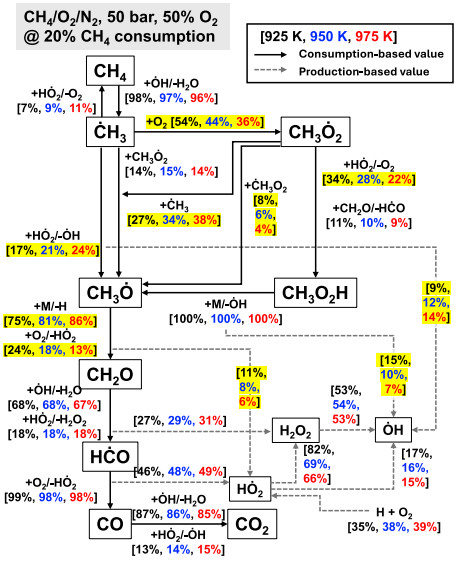



**Fig. 8.** Flux analysis on $CH_4$ oxidation at 50 bar, 50% $O_2$ and 925–975 K, at the 20% $CH_4$ consumption.

those of the other reactions (R39, R40, R121, R120, R63) increase. This indicates that the $CH_3\dot{O}_2$ chemistry is quite sensitive to temperature, and is quite important to characterize the reactivity of $CH_4$ at low temperatures.

Fig. 8 presents the results of the flux analyses at 50 bar with 50% $O_2$ at different temperatures (925–975 K). As in the case of the different $O_2$ concentrations, major changes occur upstream of $CH_2O$. However, the contribution of $\dot{C}H_3 + O_2$ (+M) = $CH_3\dot{O}_2$ (+M) to $\dot{C}H_3$ consumption decreases as the temperature increases. Subsequently, the conversion of $CH_3\dot{O}_2$ to $CH_3O_2H$ through $CH_3\dot{O}_2 + H\dot{O}_2 = CH_3O_2H + O_2$ is also weakened. This results in the decrease of the contribution of the reaction $CH_3O_2H$ (+M) = $CH_3\dot{O}$ + $\dot{O}H$ (+M) to the $\dot{O}H$ production. On the other hand, the reaction $\dot{C}H_3 + H\dot{O}_2 = CH_3\dot{O} + \dot{O}H$ is more pronounced with increasing temperature, increasing its contribution to $\dot{O}H$ radical production. These results indicate that the $CH_4$ chemistry is quite sensitive to temperature especially at low-to-intermediate temperatures.

The results obtained in the present study highlight the complexity and importance of $CH_3\dot{O}_2$ chemistry in $CH_4$ oxidation, especially under $O_2$-enriched conditions. The findings advance the application of $O_2$-enriched $CH_4$ combustion and the ignition control for practical internal combustion engines.

## 4. Conclusions

This work investigated ignition delay times (IDTs) of $O_2$-enriched $CH_4$ mixtures using a rapid compression machine (RCM). To accurately consider the facility effects in the RCM simulations for $O_2$-enriched mixtures, “pseudo” non-reactive pressure profiles were created based on reactive pressure profiles, by extrapolating an exponential decay curve in the post-EOC (end-of-compression) region. The measured IDTs become shorter as the $O_2$ concentration increases. Based on the pseudo non-reactive pressure profiles, the C3MechLiteV4.0.1 model captures the observed trends in the measured IDTs quite well regardless of the investigated $O_2$ concentrations. Further chemical reaction analyses concluded that the reactivity enhancement by $O_2$ enrichment is primarily due to the strengthened oxidation of $CH_4$ through the $CH_3\dot{O}_2$ reactions, resulting in an active production of $\dot{O}H$ via $CH_3O_2H$ (+M) = $CH_3\dot{O}$ + $\dot{O}H$ (+M). The new experimental datasets extend the benchmarks for further development of chemical kinetic mechanisms. The findings in the present study will be utilized in the application of $O_2$-enriched

$CH_4$ combustion and the ignition control for practical internal combustion engines. Future work should extend the present dataset to a broader range of operating conditions, including additional pressures and equivalence ratios.

## CRediT authorship contribution statement

**Sara Spano:** Experiment, Formal analysis, Writing – original draft. **Florian Hurault:** Experiment, Data processing, Writing – review & editing. **Fabrice Foucher:** Resources, Writing – review & editing. **Alessandro Parente:** Resources, Writing – review & editing. **Axel Coussement:** Resources, Writing – review & editing. **Francesco Contino:** Supervision, Conceptualization, Funding acquisition, Writing – review & editing. **Hervé Jeanmart:** Supervision, Funding acquisition, Writing – review & editing. **Yuki Murakami:** Numerical simulation, Software, Investigation, Formal analysis, Writing – original draft.

## Declaration of Generative AI and AI-assisted technologies in the writing process

During the preparation of this work, the authors used generative AI to proofread the article. After using this tool/service, the authors reviewed and edited the content as needed, and take full responsibility for the content of the publication.

## Declaration of competing interest

The authors declare that they have no known competing financial interests or personal relationships that could have appeared to influence the work reported in this paper.

## Acknowledgments

The authors acknowledge the funding via FEDER-RW, DECARBOWAL-TRINITHY and COGENEF–CRUCIAL. YM and AP acknowledge the Fonds de La Recherche Scientifique (FNRS) for funding via FRFS-WEL-T grant LIFETIME (WEL-T-CR-2023 A-07). The authors thank Dr. Marco Lubrano Lavadera for the insightful comments. The authors acknowledge Prof. Henry Curran and Dr. Yuxiang Zhu of University of Galway (Ireland) for the insightful discussion regarding RCM simulations.

## Appendix A. Supplementary data

Supplementary material related to this article can be found online at https://doi.org/10.1016/j.proci.2026.106758.

## References

[1] T. Pachiannan, W. Zhong, S. Rajkumar, Z. He, X. Leng, Q. Wang, A literature review of fuel effects on performance and emission characteristics of low-temperature combustion strategies, Appl. Energy 251 (2019) 113380, http://dx.doi.org/10.1016/j.apenergy.2019.113380.

[2] M. Jerome Stanley, E.G. Varuvel, M. Leenus Jesu Martin, Evaluating the potential performance of methane in lean conditions and examining the variations in combustion in a gasoline direct injection engine, Energy 302 (2024) 131838, http://dx.doi.org/10.1016/j.energy.2024.131838.

[3] J. Pan, H. Wei, G. Shu, Z. Chen, P. Zhao, The role of low temperature chemistry in combustion mode development under elevated pressures, Combust. Flame 174 (2016) 179–193, http://dx.doi.org/10.1016/j.combustflame.2016.09.012.

[4] S. Spanò, M. Savarese, A. Parente, F. Contino, H. Jeanmart, Experimental and numerical investigation of methane combustion in a HCCI engine under enriched oxygen conditions, Fuel 362 (2024) 130772, http://dx.doi.org/10.1016/j.fuel.2023.130772.

[5] P. Zhang, I.G. Zsély, V. Samu, T. Nagy, T. Turányi, Comparison of methane combustion mechanisms using shock tube and rapid compression machine ignition delay time measurements, Energy Fuels 35 (15) (2021) 12329–12351, http://dx.doi.org/10.1021/acs.energyfuels.0c04277.

[6] K. Haghighi, G.P. McTaggart-Cowan, Modelling the impacts of hydrogen–methane blend fuels on a stationary power generation engine, Energies 16 (5) (2023) 2420, http://dx.doi.org/10.3390/en16052420.

[7] B. Su, M. Papp, P. Zhang, T. Turányi, Dependence of ignition delay time on its definition – A case study on methane ignition, Combust. Flame 262 (2024) 113364, http://dx.doi.org/10.1016/j.combustflame.2024.113364.

[8] T. Qiu, H. Chen, Y. Lei, Y. Wang, A. Zhang, Study on the effect of high-pressure methane jet on lean burn laminar flame, Proc. Inst. Mech. Eng. Part D: J. Automob. Eng. 239 (8) (2025) 3132–3146, http://dx.doi.org/10.1177/09544070241254608.

[9] S. Panigrahy, A.A.E.-S. Mohamed, P. Wang, G. Bourque, H.J. Curran, When hydrogen is slower than methane to ignite, Proc. Combust. Inst. 39 (1) (2023) 253–263, http://dx.doi.org/10.1016/j.proci.2022.08.025.

[10] J.M. Harman-Thomas, D.B. Ingham, K.J. Hughes, M. Pourkashanian, Role of methyldioxy radical chemistry in high-pressure methane combustion in $CO_2$, Int. J. Chem. Kinet. 55 (10) (2023) 629–641, http://dx.doi.org/10.1002/kin.21672.

[11] M.J. Elrod, D.L. Ranschaert, N.J. Schneider, Direct kinetics study of the temperature dependence of the $CH_2O$ branching channel for the $CH_3O_2 + HO_2$ reaction, Int. J. Chem. Kinet. 33 (6) (2001) 363–376, http://dx.doi.org/10.1002/kin.1030.

[12] P.D. Lightfoot, P. Roussel, F. Caralp, R. Lesclaux, Flash photolysis study of the $CH_3O_2$ + $CH_3O_2$ and $CH_3O_2$ + $HO_2$ reactions between 600 and 719 K: unimolecular decomposition of methylhydroperoxide, J. Chem. Soc. Faraday Trans. 87 (1991) 3213–3220, http://dx.doi.org/10.1039/FT9918703213.

[13] L. Onel, et al., Kinetics and product branching ratio study of the $CH_3O_2$ self reaction, J. Phys. Chem. A 126 (9) (2022) 1592–1604, http://dx.doi.org/10.1021/acs.jpca.2c04968.

[14] F.F. Østerstrøm, et al., Kinetics of the cross-reaction of $CH_3O_2 + HO_2$ radicals, Int. J. Chem. Kinet. 55 (6) (2023) 482–495, http://dx.doi.org/10.1002/kin.21651.

[15] M. Pochet, V. Dias, B. Moreau, F. Foucher, H. Jeanmart, F. Contino, Experimental and numerical study, under LTC conditions, of ammonia ignition delay with and without hydrogen addition, Proc. Combust. Inst. 37 (1) (2019) 621–629, http://dx.doi.org/10.1016/j.proci.2018.05.138.

[16] B.W. Weber, C.-J. Sung, M.W. Renfro, On the uncertainty of temperature estimation in a rapid compression machine, Combust. Flame 162 (6) (2015) 2518–2528, http://dx.doi.org/10.1016/j.combustflame.2015.03.001.

[17] D.G. Goodwin, H.K. Moffat, I. Schoegl, R.L. Speth, B.W. Weber, Cantera: An object-oriented software toolkit for chemical kinetics, thermodynamics, and transport processes, 2023, Version 3.0.0. https://www.cantera.org.

[18] Y. Murakami, Q.-D. Wang, S. Liu, Y. Zhu, P. Wang, L.P. Maffei, R. Langer, T. Faravelli, H. Pitsch, S.J. Klippenstein, J. Bergthorson, G. Bourque, S. Wagnon, K. Senecal, H. Curran, Corrigendum to "C3MechLite: An integrated component library of compact kinetic mechanisms for low-carbon, carbon neutral and zero-carbon fuels" [Combustion and Flame 282 (2025) 114410], Combust. Flame 288 (2026) 114912, http://dx.doi.org/10.1016/j.combustflame.2026.114912.

[19] Y. Murakami, Q.-D. Wang, S. Liu, Y. Zhu, P. Wang, L.P. Maffei, R. Langer, T. Faravelli, H. Pitsch, S.J. Klippenstein, J. Bergthorson, G. Bourque, S. Wagnon, P.K. Senecal, H. Curran, C3MechLite: An integrated component library of compact kinetic mechanisms for low-carbon, carbon neutral and zero-carbon fuels, Combust. Flame 282 (2025) 114410, http://dx.doi.org/10.1016/j.combustflame.2025.114410.

[20] Y. Zhang, W. Dong, L. Vandewalle, R. Xu, G. Smith, H. Wang, Foundational Fuel Chemistry Model Version 2.0 (FFCM-2), 2023.

[21] S.J. Klippenstein, R. Sivaramakrishnan, N.J. Labbe, Y. Tao, M.P. Burke, S.N. Elliott, C.F. Goldsmith, C.R. Mulvihill, A.W. Jasper, B. Ruscic, D.H. Bross, P. Glarborg, N. Hansen, J. Zádor, J.A. Miller, Theoretically Informed Kinetics (ThInK): Establishing a modern C0-C3 mechanism for combustion modeling, Combust. Flame 282 (2025) 114501, http://dx.doi.org/10.1016/j.combustflame.2025.114501.

[22] G. Pang, D. Davidson, R. Hanson, Experimental study and modeling of shock tube ignition delay times for hydrogen–oxygen–argon mixtures at low temperatures, Proc. Combust. Inst. 32 (1) (2009) 181–188, http://dx.doi.org/10.1016/j.proci.2008.06.014.

[23] K.A. Heufer, H. Olivier, Determination of ignition delay times of different hydrocarbons in a new high pressure shock tube, Shock Waves 20 (4) (2010) 307–316, http://dx.doi.org/10.1007/s00193-010-0262-2.

[24] S. Lakshmanan, W.L. Hase, G.P. Smith, Mechanism and kinetics for the reaction of methyl peroxy radical with $O_2$, Phys. Chem. Chem. Phys. 23 (2021) 23508–23516, http://dx.doi.org/10.1039/D1CP02427B.

[25] J. Shao, R. Choudhary, D.F. Davidson, R.K. Hanson, S. Barak, S. Vasu, Ignition delay times of methane and hydrogen highly diluted in carbon dioxide at high pressures up to 300 atm, Proc. Combust. Inst. 37 (4) (2019) 4555–4562, http://dx.doi.org/10.1016/j.proci.2018.08.002.

[26] M. Karimi, B. Ochs, Z. Liu, D. Ranjan, W. Sun, Measurement of methane autoignition delays in carbon dioxide and argon diluents at high pressure conditions, Combust. Flame 204 (2019) 304–319, http://dx.doi.org/10.1016/j.combustflame.2019.03.020.